

# On the Ground State Quantum Droplet for Large Chemical Potentials

J. Holmer,<sup>1</sup> K. Z. Zhang,<sup>2</sup> and P. G. Kevrekidis<sup>3</sup>

<sup>1</sup>*Department of Mathematics, Brown University, Providence RI, 02912, USA*

<sup>2</sup>*Department of Mathematics, Northeastern University, Boston, MA, 02115, USA*

<sup>3</sup>*Department of Mathematics and Statistics, University of Massachusetts, Amherst, MA 01003-4515, USA*

In the present work we revisit the problem of the quantum droplet in atomic Bose-Einstein condensates with an eye towards describing its ground state in the large density, so-called Thomas-Fermi limit. We consider the problem as being separable into 3 distinct regions: an inner one, where the Thomas-Fermi approximation is valid, a sharp transition region where the density abruptly drops towards the (vanishing) background value and an outer region which asymptotes to the background value. We analyze the spatial extent of each of these regions, and develop a systematic effective description of the rapid intermediate transition region. Accordingly, we derive a uniformly valid description of the ground state that is found to very accurately match our numerical computations. As an additional application of our considerations, we show that this formulation allows for an analytical approximation of excited states such as the (trapped) dark soliton in the large density limit.

## I. INTRODUCTION

Over the past few years, an emerging topic in the physics of atomic Bose-Einstein condensates has been the exploration of quantum droplets. The latter constitute self-bound states arising from the interplay between the mean-field and quantum fluctuation energetic contributions [1]. In this competition, it is also important to recognize the role of the system's dimensionality [2]. Early experimental observations of the relevant settings took place in dipolar condensates [3, 4], followed shortly thereafter by trapped bosonic mixtures with contact interactions [5–7]. Such droplet states were also observed in free space, e.g., in the work of [8].

In droplet-bearing systems, the critical role of quantum fluctuations has been theoretically incorporated by means of the well-known Lee-Huang-Yang (LHY) correction term [9] that is suitably added to the standard mean-field cubic nonlinearity description [1, 10]. This leads to an extended Gross-Pitaevskii equation (EGPE) description that has been found to be fruitful for the theoretical and computational identification of such droplet patterns [11–13]. Accordingly, this formulation has been used in order to describe modulational instability and related features [14–16], collective excitations [17–20] and nonlinear wave structures in the form of solitary waves and vortices [21–27]. Indeed, already this new form of “liquid matter” has been the subject of not only numerous studies, but also relevant reviews such as [28].

In the case of the standard single-component atomic condensates (with cubic nonlinearity), the study of the system's ground state is quite mature at this stage. For the standard one-dimensional GPE, a well-known approximation is that of the Thomas-Fermi (TF) limit, which is progressively more accurate as the chemical potential is increased and consists of an inverted parabola (with compact support) [29, 30]. What is perhaps somewhat less well-known in the physics community is that while this (TF) description is accurate close to the center of the trapped 1d condensate, there have been some

significant mathematical works that have offered refinements in the vicinity of the condensate edges. In the latter, the dispersion becomes significant, creating a boundary layer which requires a more refined multiple-scales analysis to be properly captured, as has been explored in works such as those of [31, 32]. Accordingly, these works have been able to accurately approximate the relevant layer, by leveraging the so-called Hastings-McLeod solution of the Painlevé-II equation. While there exist more accurate, quasi-1d approximations of the full 3d problem [33, 34], this analysis is significant for various purposes, including towards understanding not only the asymptotics but also the excitation spectrum of the relevant ground state in an analytical (or semi-analytical/asymptotic) form.

At the present time, to the best of our knowledge, there exists no analogous analysis of the problem of the quantum droplet. In the latter case, indeed, as we will see below, the issue of the asymptotic state is further exacerbated by the attractive nature of the nonlinearity for small densities. In that light, the TF approximation fails already at a finite density and it is not possible to construct a corresponding simple-minded approximation profile by neglecting the wavefunction curvature. Accordingly, it is of interest to develop ideally a uniform approximation that allows us to capture the large chemical potential droplet wavefunction, in a way analogous to [31, 32]. This is the aim of the present work. In order to do so, we leverage a multiple-scales spatial analysis of the stationary state problem, separating the region close to the center (where the TF approximation turns out to still be valid), an intermediate, steep-descent region that we suitably quantify and finally the asymptotic decay towards the background value. Combining these 3 regions, we eventually obtain a uniform expression for the quantum droplet profile in the presence of a trap in the large chemical potential limit. This expression is of value well-beyond the strict confines of the ground state: indeed, we show that it provides us with the tools to accurately approximate excited states in the form, e.g., of the pro-

totypical dark soliton state of the trapped system.

Our presentation will be structured as follows. In section II we present the mathematical setup of the problem and our main results for the droplet system's ground state. In section III, we provide the details of our multiple-scales analysis, while in section IV we present an extension of the method for the case of the dark soliton configuration. Finally, in section V, we summarize our findings and present our conclusions, as well as some directions for future work.

## II. MATHEMATICAL SETUP & MAIN RESULT

The framework of interest to us herein will concern the homonuclear mass-balanced case of a one-dimensional (1d) bosonic mixture of two different (hyperfine) states. In line with earlier works including [24, 26, 27], we will assume that the two species feature equal self-repulsion  $g_{11} = g_{22} \equiv g$ , while across the species the attraction renders  $g_{12}$  negative. A prototypical example thereof can be encountered in the context, e.g., of  $^{39}\text{K}$ , whose states  $|1, -1\rangle$  and  $|1, 0\rangle$  have been considered previously [8] (in the 3d realm). Considering the relevant EGPE model

$$iu_t = -\frac{1}{2}u_{xx} + |u|^2u - \delta|u|u + V(x)u. \quad (1)$$

Here, we have already assumed that the energy of the system is measured in units of  $\hbar^2/(m\xi^2)$ , and  $\xi = \pi\hbar^2\sqrt{|\delta g|}/(mg\sqrt{2g})$  is the healing length, while the quantity  $\delta g = g_{12} + g$  combines the inter- and intra-species scattering lengths. Additionally, in this formulation, time, length and wave function are scaled according to  $t' = \hbar/(m\xi^2)$ ,  $x' = \xi x$  and  $u' = (2\sqrt{g})^{3/2}u/(\pi\xi(2|\delta g|)^{3/4})$ , respectively, where the primes are used for dimensional units, and the absence thereof for dimensionless units. The potential hereafter will be assumed to have a customary parabolic profile [29, 30] of the form:

$$V(x) = \frac{1}{2}\Omega^2x^2, \quad (2)$$

where  $\Omega$  represents the effective strength of the longitudinal confinement.

In what follows we will examine the steady state problem of Eq. (1) in which we will seek standing wave solutions of the form  $u(x, t) = e^{-i\mu t}q(x)$ , whose spatial profile will satisfy the steady state equation:

$$\mu q = -\frac{1}{2}q_{xx} + q^3 - \delta q^2 + V(x)q. \quad (3)$$

As is customary in the 1d setting [26], we will assume (without loss of generality for our standing solutions) that the spatial profile is real henceforth. Recall that the homogeneous steady states of the model are either  $q = 0$  or  $q = (\delta \pm \sqrt{\delta^2 + 4\mu})/2$ , with the one associated with the minus sign being modulationally unstable,

while the one with the plus sign being modulationally stable [14, 25].

Accordingly, the TF approximation in the presence of the trap replaces  $\mu$  with  $\mu - V(x)$ , which can immediately be seen to be problematic when the quantity under the radical  $\delta^2 + 4(\mu - V(x)) = 0$ , at which point the density is finite ( $q(x) = \delta/2$ ) and no continuous approximation leading to an asymptotically vanishing wavefunction can be constructed (contrary to the standard cubic GPE case). It is this conundrum that we wish to resolve through our analysis, providing an explicit spatial expression of increasing accuracy as  $\mu$  increases for the spatially confined droplet profile. The relevant branch of solutions and the approach of its "mass" (the scaled atom number) to the linear limit of the harmonic oscillator is shown in Fig. 1. The latter limit of asymptotically vanishing density pertains to the ground state of the harmonic oscillator (HO) with  $\mu \rightarrow \Omega/2$ ; recall that, more generally, the linear eigenstates of the HO have energies  $\mu = (n+1/2)\Omega$ , with the ground state pertaining to  $n = 0$ . It can be seen that the cubic GPE problem monotonically tends to this limit, as is expected from its defocusing nonlinearity, while the competing nonlinearity of the quantum droplet problem is manifested in the non-monotonic approach to the relevant limit; see also [24, 26]. In the figure, we also show a prototypical example of the TF limit for  $\mu = 1 \gg \Omega$ . Once again, for comparison the case of the standard GPE is shown (in blue thin solid line), together with the (less refined yet straightforwardly) analytically tractable inverted parabola TF approximation (blue thin dashed line). Here, we also include for the same chemical potential the numerically exact solution of the droplet problem, obtained via a fixed point iteration, compared with our analytically derived approximate profile (both in thick lines, the former in solid green, while the latter in dashed red). This clearly manifests the accuracy of our analytical approximation into which we now delve.

Changing variable

$$z = \frac{\sqrt{2}\Omega x}{\sqrt{\delta^2 + 4\mu}}, \quad w = \frac{2q - \delta}{\sqrt{\delta^2 + 4\mu}} \quad (4)$$

gives the semiclassical form:

$$0 = -\epsilon^2w_{zz} + (w^2 - f^2)(w + \sigma), \quad (5)$$

where  $f(z)^2 = 1 - z^2$  and

$$\epsilon = \frac{2\Omega}{\delta^2 + 4\mu}, \quad \sigma = \frac{\delta}{\sqrt{\delta^2 + 4\mu}}. \quad (6)$$

For  $|z| \leq 1$ , we take  $f(z) = \sqrt{1 - z^2}$ , while outside this region  $f(z) = 0$ .

For fixed  $0 < \sigma < 3$ , we determine the form of an even solution to (5) asymptotically for  $0 < \epsilon \ll 1$ . The form of the nonlinearity in (5) suggests that, in regions where  $w$  is slowly oscillating, if  $|z| \leq 1$ , we should have either  $w \approx f$ ,  $w \approx -f$ , or  $w \approx -\sigma$ . Based upon the assumption that there exists an even solution  $w$  such that  $w \approx f$

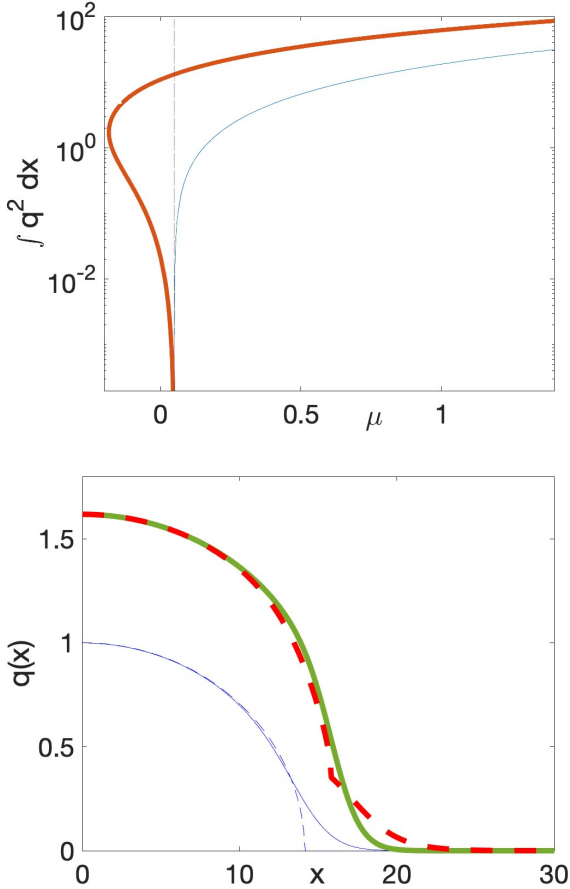


FIG. 1. (Top Panel) Typical example of the ground state branch of solutions “mass” (rescaled atom number) vs. the chemical potential  $\mu$  for a parabolic trap of strength  $\Omega = 0.1$  for the case of the cubic nonlinearity problem (standard GPE, thin blue line) vs. the quadratic-cubic nonlinearity of the present work (extended GPE, related to the droplet problem, red thick line). The vertical line denotes the linear (harmonic oscillator) limit. (Bottom panel) Prototypical example of the numerical solution (solid line) for the standard GPE (thin blue) vs. extended GPE (thick green). The analytical approximations of the Thomas-Fermi inverted parabolic profile for the former (dashed blue) and of the present work (dashed red) are also given for comparison. Here, the chemical potential is chosen as  $\mu = 1$ .

for  $|z| \ll 1$  and  $w \rightarrow -\sigma$  as  $|z| \rightarrow \infty$ , we can calculate its expected functional form. The results are as follows, with the supporting calculations given in §III.

Let  $0 < z_* < 1$  be defined as the value of  $z$  at which

$$w(z_*) = \frac{f(z_*) - \sigma}{2} \quad (7)$$

The analysis divides into three regions (see Fig 2)

- Region I,  $0 \leq z \leq z_* - O(\epsilon)$ , where  $w \approx f$ ;
- Region II,  $z_* - O(\epsilon) \leq z \leq z_* + O(\epsilon)$ , where  $w$  rapidly transitions from  $w \approx f$  to  $w \approx -\sigma$ ;

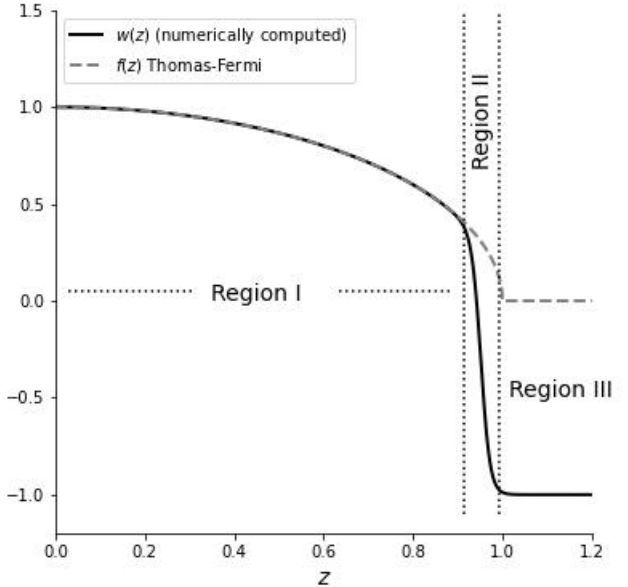


FIG. 2. The different regions of analysis, shown in the case  $\epsilon = 0.01$  and  $\sigma = 1$ . In this case,  $z_* = 0.9531$  by numerical computation.

- Region III,  $z \geq z_* + O(\epsilon)$ , where  $w \approx -\sigma$ .

The asymptotic description of  $z_*$  and  $w$ , derived in §III, that is uniformly valid in Regions I, II and III, is:

$$z_* = z_0 + \frac{3\sqrt{2}}{4\sigma} \epsilon + O(\epsilon^2) \quad (8)$$

where  $z_0 = \sqrt{1 - \frac{\sigma^2}{9}}$  (so that  $f_0 = f(z_0) = \sigma/3$ ) and

$$w(z) = \frac{f(z) - \sigma}{2} - \frac{f(z) + \sigma}{2} \tanh \left( \frac{2\sigma}{3\sqrt{2}} \frac{z - z_*}{\epsilon} \right) \quad (9)$$

As stated above, the result is derived for fixed  $0 < \sigma < 3$  as an asymptotic expansion for  $\epsilon \searrow 0$ . To determine a practical range of applicability, note that Region II should be situated strictly inside  $|z| \leq 1$ . Taking  $z_*$  as given by (8), this converts to the condition

$$\epsilon < \frac{4\sigma}{3\sqrt{2}} \left( 1 - \sqrt{1 - \frac{\sigma^2}{9}} \right)$$

When (8), (9) are converted using (4), (6), the result takes the form

$$x_* = \frac{1}{\sqrt{2}\Omega} \sqrt{\frac{8\delta^2}{9} + 4\mu} + \frac{1}{2} + O(\Omega) \quad (10)$$

and

$$u(x) = \frac{1}{4} (\delta + \sqrt{\delta^2 + 4\mu - 2\Omega^2 x^2}) \left( 1 - \tanh \left( \frac{\delta(x - x_*)}{3} \right) \right) \quad (11)$$

In this form, the result can be interpreted as an asymptotic expansion for  $\mu, \delta = O(1)$  and  $0 < \Omega \ll 1$ . The effective range of applicability converts to

$$\Omega < \sqrt{2} \left( \sqrt{\delta^2 + 4\mu} - \sqrt{\frac{8\delta^2}{9} + 4\mu} \right). \quad (12)$$

The upper bound (12) allows for a comparison to the case  $\delta = 0$  studied by [31]. For  $\mu = O(1)$ , as  $\delta \searrow 0$ , (12) becomes  $\Omega < \frac{2\delta^2}{9\sqrt{2}\mu}$ , showing that  $\Omega$  is pinched to zero in this limit. Indeed,  $x_*$  is approaching the boundary of the TF layer, and the refined Painlevé II asymptotics of [31] are needed for a more accurate description.

### III. DETAILED ANALYSIS

To justify (8), (9), define  $\phi$  via the equation

$$w = \frac{f - \sigma}{2} - \frac{f + \sigma}{2}\phi \quad (13)$$

Let  $y = (z - z_0)/\epsilon$ . In this reference frame, Region I corresponds to  $y \ll -1$ , Region II lies in  $-1 \lesssim y \lesssim 1$ , and Region III corresponds to  $y \gg 1$ . Comparing (7) and (13), we see that  $z_*$  is characterized as the  $z$ -value at which  $\phi(z_*) = 0$ .

In Region I,  $w \approx f$ , so that in view of (13), we fix the  $y \rightarrow -\infty$  boundary conditions as

$$\phi \rightarrow -1, \quad \phi_y \rightarrow 0 \quad \text{as } y \rightarrow -\infty \quad (14)$$

In Region III,  $w \approx -\sigma$ , so in view of (13), we set the  $y \rightarrow +\infty$  boundary conditions as

$$\phi \rightarrow 1, \quad \phi_y \rightarrow 0 \quad \text{as } y \rightarrow +\infty \quad (15)$$

By assuming that the boundary conditions (14), (15) hold up to second order in  $\epsilon$ , we will be able to obtain a consistent expansion, as follows.

Plugging (13) into (5) and changing variable  $y \mapsto \xi$ , with

$$\frac{d\xi}{dy} = \frac{f + \sigma}{2\sqrt{2}} \quad \xi = 0 \leftrightarrow y = 0 \quad (16)$$

leads to the transformed equation

$$\begin{aligned} \phi_{\xi\xi} + 2(1 - \phi^2)(\phi - h) \\ = -\epsilon \frac{12f_z}{\sqrt{2}(f + \sigma)^2} \phi_\xi + \epsilon^2 \frac{8f_{zz}}{(f + \sigma)^3} (1 - \phi) \end{aligned} \quad (17)$$

where  $h = (3f - \sigma)/(f + \sigma)$ . Multiplying (17) by  $\phi_\xi$  and integrating gives

$$H(\phi, \phi_\xi) \Big|_{\xi=-\infty}^{\xi=+\infty} = \int_{-\infty}^{+\infty} R(\xi) d\xi \quad (18)$$

where

$$\begin{aligned} H(\phi, \phi_\xi) &= \frac{1}{2}\phi_\xi^2 + \phi^2 - \frac{1}{2}\phi^4 \\ R &= 2h(1 - \phi^2)\phi_\xi - \epsilon \frac{12f_z}{\sqrt{2}(f + \sigma)^2} \phi_\xi^2 \end{aligned} \quad (19)$$

For the boundary values (14), (15), the left side of (18) is zero.

The equation (17) is still an exact representation of (5), but at this point we initiate an asymptotic expansion. In order that the right side of (18) vanish at zero order in  $\epsilon$ , we need  $h = O(\epsilon)$ . Setting  $h = 0$  and dropping the right side of (17), it becomes  $0 = \phi_{\xi\xi} + 2(1 - \phi^2)\phi$ , which has the solution

$$\phi(\xi) = \tanh(\xi - \xi_1), \quad (20)$$

where  $\xi_1$  is an undetermined shift. Setting  $h = 0$  is equivalent to setting  $f = \sigma/3$ . Let

$$z_0 = \sqrt{1 - \frac{\sigma^2}{9}} \iff f(z_0) = \frac{\sigma}{3}.$$

With  $z_0$  as a point of reference, the asymptotic form of (16) is:

$$y = \frac{2\sqrt{2}}{f_0 + \sigma} \xi + O(\epsilon)\xi^2 = \frac{3\sqrt{2}}{2\sigma} \xi + O(\epsilon)\xi^2 \quad (21)$$

The expansion of  $h$  is

$$h = -\epsilon \frac{81\sqrt{2}z_0}{8\sigma^3} \xi + O(\epsilon^2)\xi^2$$

This and using and (20) as an approximation for  $\phi$  in (19) provides an expansion for  $R$ :

$$R = -\epsilon \frac{81z_0}{2\sqrt{2}\sigma^3} (\xi - \frac{1}{2}) \operatorname{sech}^4(\xi - \xi_1) + O(\epsilon^2)$$

Substituting this into the right side of (18) (with left side = 0) implies that  $\xi_1 = \frac{1}{2} + O(\epsilon)$  in order that the right side of (18) vanish at first order in  $\epsilon$ .

Substituting (21) into  $y = (z - z_0)/\epsilon$ , we obtain

$$z = z_0 + \epsilon \frac{3\sqrt{2}}{2\sigma} \xi + O(\epsilon^2)\xi^2 \quad (22)$$

Recall that  $z_*$  is characterized as the  $z$ -value at which  $\phi(z_*) = 0$ . By (20), this corresponds to  $\xi = \xi_1$  and thus

$$z_* = z_0 + \epsilon \frac{3\sqrt{2}}{2\sigma} \xi_1 + O(\epsilon^2) \quad (23)$$

which gives (8). From (20), we can replace  $\phi$  with  $\tanh$  in (13) and also use the difference of (22) and (23) to reexpress  $\xi - \xi_1$ , in order to obtain (9).

#### IV. AN EXTENSION: DARK SOLITONS

Having constructed a uniform approximation to the ground state of the quantum droplet model in the large  $\mu$  limit, we now turn to an interesting extension of the relevant waveform. In particular, it is well-known that for the standard GPE model, the excited states in the form of dark solitons can be well-approximated in the large density (large chemical potential) limit by the ground TF state multiplied by the dark soliton of the homogeneous equation [35]. A relevant example for chemical potential  $\mu = 1$  and  $\Omega = 0.1$  is shown in the bottom panel of Figure 3. The central portion of the corresponding one-soliton stationary, anti-symmetric excited state wavefunction (the so-called black soliton [36]) is very well approximated by  $\tanh(x)$ , while the remaining waveform, aside from the boundary layer discussed in section I, is well approximated by the TF profile.

It is then natural to expect that a similar strategy can be used to *analytically* approximate, in a uniform way, black solitons in the quantum droplet model, which have been the subject of intense recent research efforts [24, 26, 27]. In particular, we leverage the analytical approximation of Eq. (11) for the ground state and multiply the relevant spatial profile by the exact analytical dark soliton of the homogeneous quantum droplet setting, as derived in [26]. Indeed, we use a similar notation as that work labeling  $q_+ = (\delta + \sqrt{\delta^2 + 4\mu})/2$  and expressing the black soliton as:

$$u_{\text{dark}}(x) = q_+ + \frac{-\mathcal{B}(\mu) + \sqrt{\mathcal{B}^2(\mu) - 4\mathcal{A}(\mu)\mathcal{C}(\mu)}}{2\mathcal{A}(\mu)}, \quad (24)$$

in which expression the symbols  $\mathcal{A}$ ,  $\mathcal{B}$  and  $\mathcal{C}$  are given by:  $\mathcal{A}(\mu) = B^2 - 4A \tanh^2(\sqrt{A}(x))$ ,  $\mathcal{B}(\mu) = 4AB \operatorname{sech}^2(\sqrt{A}(x))$ , and  $\mathcal{C}(\mu) = 4A^2 \operatorname{sech}^2(\sqrt{A}(x))$ , with  $A = 4\mu + (1 + \sqrt{1 + 4\mu})$  and  $B = 2(\frac{1}{3} + \sqrt{1 + 4\mu})$ . It is important to recall that the expression of Eq. (24) can be used only for  $x$  such that  $u_{\text{dark}} > 0$ , while the profile is supposed to be anti-symmetric around the point of zero crossing. Notice that also the point of zero crossing in the homogeneous model can be shifted at will due to the translational invariance of the underlying setting. By centering the relevant dark soliton around the center of the trap, as is expected for the stationary trapped black soliton state, and multiplying it by Eq. (11), we observe in the bottom panel of Fig. 3 that we get a very accurate approximation (thick dashed line) to the full numerical result (thick solid line). This happens for large chemical potentials ( $\mu \gg \Omega$ ) for the branch of dark solitary wave solutions that is shown in the top panel of the figure, once again compared between the GPE and the EGPE models, in order to observe the impact of the attractive (beyond-mean-field) nonlinear term in the latter. This, in turn, can be the basis for analyses similar to those of [35] that may enable the systematic characterization of excited (multiple dark solitary wave) states stability and dynamics. We comment on this possibility further in the next section.

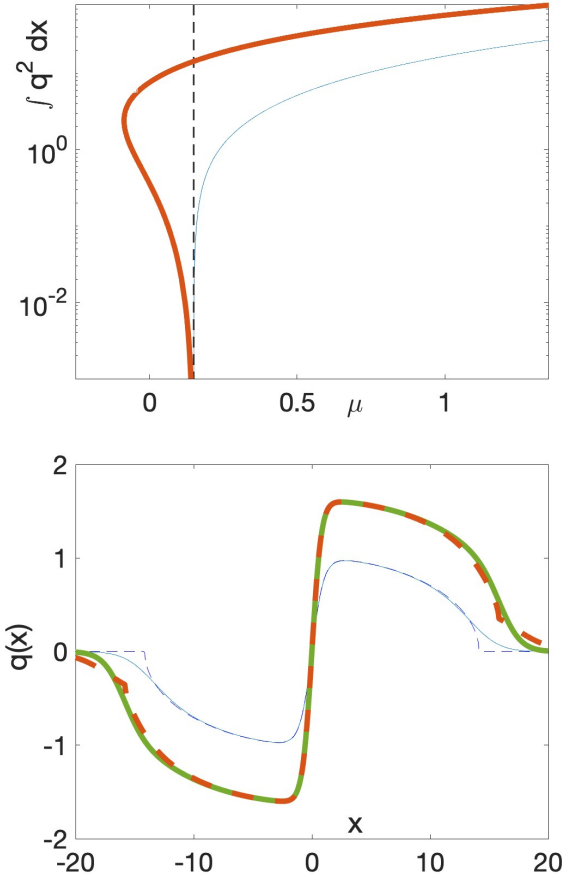


FIG. 3. (Top panel) Similar to Figure 1, but now for the prototypical dark soliton structure. Once again, the trap strength is  $\Omega = 0.1$ , hence the linear limit of the (harmonic oscillator) first excited state lies at  $\mu = 3\Omega/2 = 0.15$ . The thin blue line of the GPE is compared to the red thick line of the droplet case dark soliton branch continuation. (Bottom panel) Comparison of the respective dark solitons. The thin blue lines reflect the GPE result: here, the solid line shows the numerical dark soliton, while the dashed one represents the Thomas-Fermi approximation multiplied by the  $\tanh$  soliton profile. The respective droplet model states, also for  $\mu = 1$  (as in the GPE) are shown by thick lines, with the analytical (dashed line) state arising from the multiplication of Eq. (11) by the analytical solitary wave of Ref. [26].

#### V. CONCLUSIONS AND FUTURE CHALLENGES

In this work we have analyzed the ground state of the extended Gross-Pitaevskii equation in the presence of a parabolic confinement in the regime of the so-called Thomas-Fermi limit, i.e., for the case of large densities/chemical potentials. We combined a separation of the spatial domain into different regions (the central region, the rapid transition —interface— region and the asymptotic state region) along with an analysis of each one through suitable rescalings and asymptotic methods

in order to extract a uniformly valid asymptotic formula that we tested again in direct numerical computations via fixed point iteration methods to provide an increasingly accurate description of the quantum droplet in the large density regime.

Naturally, this development paves the way for a number of possible considerations for the future. On the one hand, this naturally poses the question of whether approximate excitation frequencies for the quantum droplet can be extracted in this limit, by analogy of what has been done for the case of the standard GPE; see, e.g., the discussion of [37]. On the other hand, the availability of such an analytical “ansatz” for a TF solution may offer the backdrop for the consideration of the asymptotic form of higher excited states, such as multiple dark solitons, in analogy with earlier works that were able to derive effective particle equations for such coherent structures [38].

At the same time, such analysis can provide a starting point for the consideration of higher dimensional analogues of the model and the asymptotic analysis of both droplet, but also importantly vortical patterns therein [21, 25]. Such studies are currently in progress and will be presented in future publications.

## ACKNOWLEDGMENTS

This material is based upon work supported by the U.S. National Science Foundation under the awards PHY-2110030 and DMS-2204702 (PGK), and DMS-2055072 (JH). PGK gratefully acknowledges numerous insightful discussions with S.I. Mistakidis, G.C. Katsimiga, R. Carretero-González, S. Chandramouli B.A. Malomed, G.N. Koutsokostas and D.J. Frantzeskakis on the subject of quantum droplets.

- 
- [1] D. S. Petrov, Phys. Rev. Lett. **115**, 155302 (2015).
  - [2] A. Khan and A. Debnath, Frontiers in Physics , 534 (2022).
  - [3] M. Schmitt, M. Wenzel, F. Böttcher, I. Ferrier-Barbut, and T. Pfau, Nature **539**, 259 (2016).
  - [4] L. Chomaz, I. Ferrier-Barbut, F. Ferlaino, B. Laburthe-Tolra, B. L. Lev, and T. Pfau, Rep. Progr. Phys. (2022).
  - [5] C. R. Cabrera, L. Tanzi, J. Sanz, B. Naylor, P. Thomas, P. Cheiney, and L. Tarruell, Science **359**, 301 (2018).
  - [6] P. Cheiney, C. R. Cabrera, J. Sanz, B. Naylor, L. Tanzi, and L. Tarruell, Phys. Rev. Lett. **120**, 135301 (2018).
  - [7] C. D’Errico, A. Burchianti, M. Prevedelli, L. Salasnich, F. Ancilotto, M. Modugno, F. Minardi, and C. Fort, Phys. Rev. Research **1**, 033155 (2019).
  - [8] G. Semeghini, G. Ferioli, L. Masi, C. Mazzinghi, L. Wolswijk, F. Minardi, M. Modugno, G. Modugno, M. Inguscio, and M. Fattori, Phys. Rev. Lett. **120**, 235301 (2018).
  - [9] T. D. Lee, K. Huang, and C. N. Yang, Phys. Rev. **106**, 1135 (1957).
  - [10] D. S. Petrov and G. E. Astrakharchik, Phys. Rev. Lett. **117**, 100401 (2016).
  - [11] G. Ferioli, G. Semeghini, S. Terradas-Briansó, L. Masi, M. Fattori, and M. Modugno, Phys. Rev. Research **2**, 013269 (2020).
  - [12] C. Fort and M. Modugno, Applied Sciences **11** (2021), 10.3390/app11020866.
  - [13] S. Mistakidis, A. Volosniev, R. Barfknecht, T. Fogarty, T. Busch, A. Foerster, P. Schmelcher, and N. Zinner, Physics Reports **1042**, 1 (2023), few-body Bose gases in low dimensions—A laboratory for quantum dynamics.
  - [14] T. Mithun, A. Maluckov, K. Kasamatsu, B. A. Malomed, and A. Khare, Symmetry **12**, 174 (2020).
  - [15] T. Mithun, S. I. Mistakidis, P. Schmelcher, and P. G. Kevrekidis, Phys. Rev. A **104**, 033316 (2021).
  - [16] S. R. Otajonov, E. N. Tsot, and F. K. Abdullaev, Phys. Rev. A **106**, 033309 (2022).
  - [17] M. Tylutki, G. E. Astrakharchik, B. A. Malomed, and D. S. Petrov, Phys. Rev. A **101**, 051601(R) (2020).
  - [18] I. A. Englezos, S. I. Mistakidis, and P. Schmelcher, Phys. Rev. A **107**, 023320 (2023).
  - [19] P. Stürmer, M. N. Tengstrand, R. Sachdeva, and S. M. Reimann, Phys. Rev. A **103**, 053302 (2021).
  - [20] A. Cappellaro, T. Macrì, and L. Salasnich, Phys. Rev. A **97**, 053623 (2018).
  - [21] Y. Li, Z. Chen, Z. Luo, C. Huang, H. Tan, W. Pang, and B. A. Malomed, Phys. Rev. A **98**, 063602 (2018).
  - [22] S. Gangwar, R. Ravishankar, P. Muruganandam, and P. K. Mishra, Phys. Rev. A **106**, 063315 (2022).
  - [23] Y. V. Kartashov, V. M. Lashkin, M. Modugno, and L. Torner, New J. Phys. **24**, 073012 (2022).
  - [24] M. Edmonds, Phys. Rev. Res. **5**, 023175 (2023).
  - [25] S. Saqlain, T. Mithun, R. Carretero-González, and P. G. Kevrekidis, Phys. Rev. A **107**, 033310 (2023).
  - [26] G. C. Katsimiga, S. I. Mistakidis, G. N. Koutsokostas, D. J. Frantzeskakis, R. Carretero-González, and P. G. Kevrekidis, Phys. Rev. A **107**, 063308 (2023).
  - [27] G. C. Katsimiga, S. I. Mistakidis, B. A. Malomed, D. J. Frantzeskakis, R. Carretero-Gonzalez, and P. G. Kevrekidis, Condensed Matter **8** (2023), 10.3390/condmat8030067.
  - [28] Z. Luo, W. Pang, B. Liu, Y. Li, and B. A. Malomed, Frontiers of Physics **16**, 32201 (2021).
  - [29] C. J. Pethick and H. Smith, *Bose-Einstein condensation in dilute gases* (Cambridge university press, 2008).
  - [30] S. Stringari and L. Pitaevskii, *Bose-Einstein Condensation* (Oxford University Press, Oxford, United Kingdom, 2003).
  - [31] C. Gallo and D. E. Pelinovsky, Asymptot. Anal. **73**, 53 (2009).
  - [32] G. Karali and C. Sourdis, Archive for Rational Mechanics and Analysis **217**, 439 (2015).
  - [33] L. Salasnich, A. Parola, and L. Reatto, Phys. Rev. A **65**, 043614 (2002).
  - [34] A. M. n. Mateo and V. Delgado, Phys. Rev. A **77**, 013617 (2008).
  - [35] M. P. Coles, D. E. Pelinovsky, and P. G. Kevrekidis, Nonlinearity **23**, 1753 (2010).

- [36] D. J. Frantzeskakis, *J. Phys. A: Math. and Th.* **43**, 213001 (2010).
- [37] P. G. Kevrekidis and D. E. Pelinovsky, *Phys. Rev. A* **81**, 023627 (2010).